Manuscript submitted to
AIMS' Journals
Volume **X**, Number **0X**, XX **200X**

doi:10.3934/xx.xx.xx.xx

pp. **X–XX**

ON THE NODAL SET OF THE EIGENFUNCTIONS OF THE LAPLACE-BELTRAMI OPERATOR FOR BOUNDED SURFACES IN $\mathbb{R}^3$: A COMPUTATIONAL APPROACH

Andrea Bonito

Department of Mathematics, Texas A&M University
College Station, TX 77845, USA

Roland Glowinski

Department of Mathematics, University of Houston
Houston, TX 77204-3008, USA

To the memory of I.M. Visik

Abstract. In this article we investigate, via numerical computations, the intersection properties of the nodal set of the eigenfunctions of the Laplace-Beltrami operator for smooth surfaces in $\mathbb{R}^3$ (the nodal set of a continuous function is the set of those points at which the function vanishes). First, we briefly discuss the numerical solution of the eigenvalue/eigenfunction problem for the Laplace-Beltrami operator on bounded surfaces of $\mathbb{R}^3$, and then consider some specific surfaces and visualize how the nodal lines intersect (or not) depending of the symmetries verified by the surface. After validating our computational methodology with the surface of a ring torus, we will investigate a simple surface without symmetry and observe that in that case the nodal set of the computed eigenfunctions consists of non intersecting lines, suggesting some conjecture. We observe also that for the above symmetry-free surface, the number of connected components of the nodal set varies non-monotonically with the rank of the associated eigenvalue (assuming that the eigenvalues are ordered by increasing value).

1. **Introduction.** While visiting the Universidad autónoma metropolitana in Mexico-City several years ago, one of the authors was asked to investigate computationally the following question:

Do the nodal lines - the lines where a function vanishes - of the solutions of a particular family of two-dimensional nonlinear eigenvalue problems for elliptic operators, intersect orthogonally the boundary $\partial\Omega$ if the domain Ω, where the problem is "taking place", is without symmetry?

Computations done in 2006 [9, 8] suggest that indeed the nodal lines intersect orthogonally $\partial\Omega$. The *nonlinear eigenvalue* problem in question was:

$$\left\{ \begin{array}{rcll} -\Delta u & = & \lambda u^3 & \text{in } \Omega, \\ u & = & 0 & \text{on } \partial\Omega, \end{array} \right. \tag{1}$$

2010 *Mathematics Subject Classification.* Primary: 65N30, 65N25.

Key words and phrases. Laplace-Beltrami Operator, Eigenpair, Nodal Lines, Finite Element Methods, Surfaces.

The first author is partially supported by NSF grant DMS-1254618, the second author is partially supported by NSF grant DMS-0913982.

with $\lambda \geq 0$.

Motivated by problem (1), it is natural to consider related questions for bounded surfaces of $\mathbb{R}^3$. We start the investigations with a "simple" linear operator, namely the Laplace-Beltrami (or surface Laplacian) operator, and determine if, and how, the nodal lines of the eigenfunctions of the above linear operator intersect. Although our initial motivation was not driven by applications outside mathematics, it is worth noting that the "geography" of the nodal lines associated with the Laplace-Beltrami operator seem to provide a powerful tool to analyze MRI pictures of the brain (and of the colon) (see [12] and the references therein). This article briefly discusses the numerical solution of the eigenvalue/eigenfunction problem for the Laplace-Beltrami operator on bounded surfaces of $\mathbb{R}^3$, and then visualizes how the nodal lines intersect (or do not) depending of the symmetries verified by the surface. Our numerical investigation suggests that they do not intersect in the absence of symmetries. Interesting enough, when some symmetry is added to the surface, the nodal lines may intersect. This numerical study raises some mathematical questions regarding the topology of the nodal sets (surface without the nodal lines).

As a final comment, let us mention that the distribution of the nodal lines provides useful information on the position of the actuators if one wants to control a diffusion process taking place on a surface: the more symmetries the surface has the more expansive the control will be, the sphere being clearly the worst surface from that point of view (for the Laplace-Beltrami operator).

2. The Eigenvalue/Eigenfunction Problem for the Laplace-Beltrami Operator.

Let us consider a *smooth bounded* surface σ of $\mathbb{R}^3$ *without boundary*. Our goal here is to investigate the influence of *symmetries* on the *intersection properties* of the nodal lines of the *eigenfunctions* of the *Laplace-Beltrami operator*, namely of the functions u_λ, where $(\lambda, u_\lambda) \in \mathbb{R}_+ \times H^1(\sigma)$ satisfies

$$\begin{cases} \displaystyle\int_\sigma \nabla_\sigma u_\lambda \cdot \nabla_\sigma v \; d\sigma = \lambda \int_\sigma u_\lambda v \; d\sigma, \qquad \forall v \in H^1(\sigma), \\ \displaystyle\int_\sigma |u_\lambda|^2 \; d\sigma = 1. \end{cases} \tag{2}$$

Here ∇_σ is the tangential gradient on σ and

$$H^1(\sigma) := \left\{ v \in L_2(\sigma) \mid \int_\sigma |\nabla_\sigma v|^2 \; d\sigma < +\infty \right\}.$$

Notice that the pair $(0, |\sigma|^{-1/2})$ is an obvious solution of (2), where $|\sigma|$ denotes the area of σ.

Suppose that (λ, u_λ) is a solution of (2), the *nodal set* is defined as the set $u_\lambda^{-1}(0)$. Every connected component of the set $\sigma \setminus u_\lambda^{-1}(0)$ is called a *nodal domain* of u_λ and the number of nodal domains is called the nodal number of u_λ. Results on the mathematical properties of the nodal set can be found in [14, 6] (see also the references therein). In particular, the nodal number of the nth eigenfunction is $\leq n+1$ and, modulo a small perturbation of σ if necessary, the nodal number is 2 (the nodal lines do not intersect generically).

3. Numerical Approximations.

3.1. **Parametric Finite Element Methods on Surfaces.** The solution of the linear eigenvalue problem (2) is numerically approximated using a parametric finite element method described briefly now. We start with a polyhedral surface Σ approximating σ. The facets of Σ are assumed to be quadrilaterals and we denote by $\mathcal{T}$ the set of these quadrilaterals. Each quadrilateral $T \in \mathcal{T}$ is described by a non-degenerate bi-linear parametrization $\mathcal{F}_T : \widehat{T} \to T$, where $\widehat{T} := (0,1) \times (0,1) \subset \mathbb{R}^2$. We define the finite dimensional space $\mathbb{V}(\mathcal{T}) \subset H^1(\Sigma)$ by

$$\mathbb{V}(\mathcal{T}) := \Big\{ V : C^0(\Sigma) \to \mathbb{R} \mid \forall T \in \mathcal{T},\ \exists \widehat{V}_T : \widehat{T} \to \mathbb{R} \text{ bi-linear and such that } V|_T = \widehat{V}_T \circ \mathcal{F}_T^{-1} \Big\}.$$

Using these notations, the discrete counterpart of (2) reads: Seek $(\Lambda, U_\Lambda) \in \mathbb{R}_+ \times \mathbb{V}(\mathcal{T})$ such that

$$\begin{cases} \displaystyle\sum_{T\in\mathcal{T}} \int_T \nabla_T U_\Lambda \cdot \nabla_T V \, d\Sigma = \Lambda \sum_{T\in\mathcal{T}} \int_T U_\Lambda V \, d\Sigma, \qquad \forall V \in \mathbb{V}(\mathcal{T}), \\ \displaystyle\sum_{T\in\mathcal{T}} \int_T |U_\Lambda|^2 \, d\Sigma = 1. \end{cases} \tag{3}$$

Notice that to help the reader, we use capital letters to denote numerical approximations; compare to (2).

Taking advantage of the parametric representation of the surface Σ, the surface gradients are given on $\widehat{T}$ by

$$(\nabla_T v) \circ \mathcal{F}_T = D\mathcal{F}_T \; G_T^{-1} \widehat{\nabla}(v \circ F_T), \tag{4}$$

where

$$D\mathcal{F}_T := \left(\frac{\partial}{\partial \widehat{x}_j} (\mathcal{F}_T)_i \right)_{i=1,j=1}^{3,2} : \widehat{T} \to \mathbb{R}^{3\times 2}$$

is the derivative of $\mathcal{F}_T$,

$$G_T := (D\mathcal{F}_T)^t (D\mathcal{F}_T) : \widehat{T} \to \mathbb{R}^{2\times 2}$$

is the first fundamental form and $\widehat{\nabla} := \left(\frac{\partial}{\partial \widehat{\mathbf{x}}_1}, \frac{\partial}{\partial \widehat{\mathbf{x}}_2} \right)^t$ is the standard gradient in $\mathbb{R}^2$.

Remark 1 (Numerical Implementation)**.** Relation (4) is a generalization to surfaces of the standard implementation of the finite element methods and is therefore easily implementable. We refer to [5] for a discussion on its implementation within the *deal.ii* library [1]. In fact, given a basis $\{\varphi_i\}_{i=1}^N$ of $\mathbb{V}(\mathcal{T})$ with $N := \dim(\mathbb{V}(\mathcal{T}))$, system (3) takes the following algebraic form

$$A[U] = \Lambda M[U], \qquad [U]^t M[U] = 1, \tag{5}$$

where $A, M \in \mathbb{R}^{N\times N}$ are defined componentwise by

$$A_{i,j} := \sum_{T\in\mathcal{T}} \int_{\widehat{T}} \left(\widehat{\nabla}(\varphi_j \circ F_T) \right)^t G_T^{-1} \left(\widehat{\nabla}(\varphi_i \circ F_T) \right) \sqrt{\det(G_T)},$$

$$M_{i,j} := \sum_{T\in\mathcal{T}} \int_{\widehat{T}} (\varphi_j \circ F_T)(\varphi_i \circ F_T) \sqrt{\det(G_T)}$$

and $[U]$ is the vector of $\mathbb{R}^N$ whose components are coefficients of the solution U of problem (3) corresponding to the basis $\{\varphi_i\}_{i=1}^N$.

We conclude this section by noting that two different sources of error inherent to (3) need to be accounted for: a *partial differential equation error* due to the approximation by U_Λ of the solution to (2) with σ replaced by the approximate surface Σ and a *geometric error* related to the approximation of σ by Σ (note that $U_\Lambda \in \mathbb{V}(\mathcal{T}) \subset H^1(\Sigma)$ not $H^1(\sigma)$). We refer to [7, 2] for more details.

4. Numerical Observations.

The finite dimensional symmetric eigenvalue problems (5) is solved within the *deal.ii* library [1] by an eigenvalue/eigenvector solver from SLEPc [11] (for Scalable Library for Eigenvalue Problem Computations) developed at the Polytechnic University of Valencia (Spain). This solver relies on Krylov iterations, preconditioned by a multi-level algorithm developed by the first author and J. Pasciak for the solution of linear second order elliptic problems on surfaces (see [4] for details).

4.1. Presentation of Test Problems.

We consider three surfaces, namely:

1. The surface (denoted by σ_1 here) of a ring torus of aspect ratio 4/3. We choose this particular aspect ratio for comparison purpose since it was also considered in [10]. In the latter work, finite differences on triangular subdivisions are employed together with the ARPACK eigensolver [13].
2. The surface σ_2 of equation
$$50xyz\left(1-\frac{x}{2}-\frac{y}{3}-\frac{z}{5}\right)=1 \tag{6}$$
contained in the *first octant* of $\mathbb{R}^3$ (i.e., $x, y, z > 0$); unlike σ_1, this surface is *without symmetries* implying that the *eigenvalues* are of *multiplicity one* for the Laplace-Beltrami operator. In addition, σ_2 cannot be parametrized via one single local coordinate system, thereby justifying our parametric approach.
3. For comparison with σ_2, we consider the symmetric surface σ_3 of equation
$$1024xyz\,(1-x-y-z)=1, \qquad x,y,z>0. \tag{7}$$
As we shall see, in this context, some nodal lines may intersect.

4.2. Numerical Results for σ_1.

We insist one more time that we took this example mostly for validation purposes and compare our results with those in [10]. Notice however that the eigenvalue system is obtained by a quite different approach in [10], which contains in addition a discussion on the influence of the torus aspect ration in the eigenvalues multiplicity. All the results reported below have been obtained using a finite element mesh with $262,144$ vertices (computations with a twice finer mesh produce very close results, for the first ten eigenvalues at least) and are in excellent agreement with the results provided in [10].

The following was observed:

- The first non-zero eigenvalue is of multiplicity 2 (as are many others) while the following one is of multiplicity 1. The nodal lines of the associated computed eigenfunctions have been visualized on Figures 1 and 2. They suggest that the nodal number of the continuous eigenfunctions is 2.
- When the nodal lines intersect, they do so orthogonally as expected. Figure 3 depicts the nodal lines associated with the 5th distinct eigenvalue (of multiplicity 2). The nodal number of the associated eigenfunction is 4.

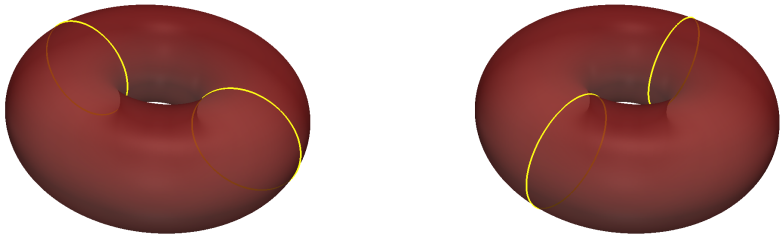

FIGURE 1. Surface Σ_1. Nodal lines of two eigenfunctions associated with the 1st non-zero eigenvalue (of multiplicity 2). The nodal lines do not intersect.

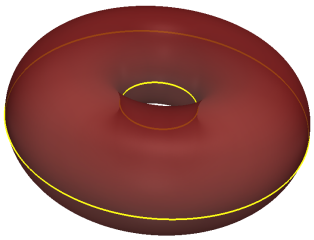

FIGURE 2. Surface Σ_1. Nodal lines of an eigenfunctions associated with the 2nd non-zero eigenvalue (of multiplicity 1). The nodal lines do not intersect.

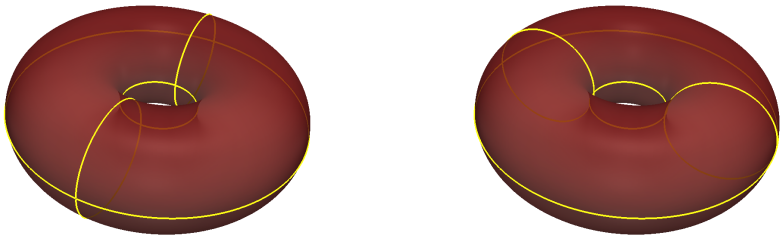

FIGURE 3. Surface Σ_1. Nodal lines of two eigenfunctions associated with the 5th non-zero eigenvalue (of multiplicity 2). The nodal lines intersect orthogonally.

4.3. **Numerical Results for σ_2.** The first issue to address is the construction of an approximation Σ_2 of σ_2 given by equation (6). We proceed as follows:

1. Let $\widehat{\Sigma}_2$ be the tetrahedron whose vertices are $\{0,0,0\}$, $\{2,0,0\}$, $\{0,3,0\}$, $\{0,0,5\}$, and denote by $G := \{1/2, 3/4, 5/4\}$ their barycenter; each facet of the boundary $\partial\widehat{\Sigma}_2$ of $\widehat{\Sigma}_2$ is a triangle.

2. Each facet is decomposed in 3 quadrilaterals using the midpoints of the facet edges and the facet barycenter, see Figure 4. The collection of all quadrilaterals obtained is the base subdivision $\widehat{\mathcal{T}}_0$.
3. Quad-refine $\widehat{\mathcal{T}}_0$ (see e.g. [3, Section 6.3]) to increase the solution as desired. The resulting subdivision is denoted $\widehat{\mathcal{T}}$.
4. The grid points of the mesh on Σ_2 are obtained by taking the intersection of σ_2 with the half-lines joining G to the grid points of $\widehat{\mathcal{T}}$. This requires the numerical solution of N quartic equations of one variable, N being the total number of grid points; we used Newton's method for these computations.

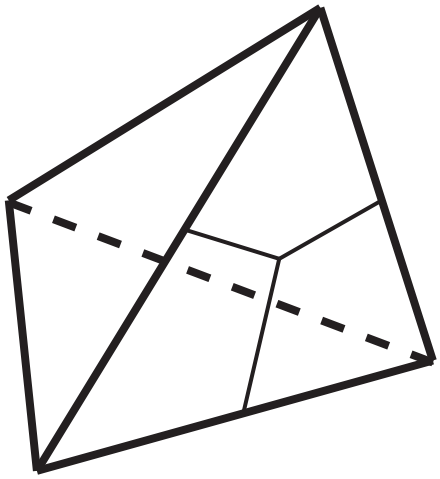

FIGURE 4. Generation of Σ_2 (step 2): Initial tetrahedron $\widehat{\Sigma}_2$ (in bold). Each facet is subdivided in 3 quadrilaterals using the midpoints of the facet edges vertices and the facet barycenter.

Remark 2 (Triangulation)**.** To achieve an approximating surface Σ_2 made of triangles, one can proceed as above skipping step 3 and replacing quad-refinement by any process generating triangles.

The use of quadrilateral finite element methods for solving second order linear elliptic problems on surfaces of $\mathbb{R}^3$ is discussed in [2]. The design and study of multilevel methods in this context is proposed in [4]. A quadrilateral based finite element mesh with $49,152$ grid points (and elementary quadrilaterals), which corresponds to 6 uniform quad-refinements in step 3 described above, has been visualized on Figure 5. We observe the quasi-uniformity of the mesh shown.

The results presented below concern the first thirty non-zero eigenvalues; they have been obtained with the mesh visualized in Figure 5; the results obtained with a mesh twice finer are essentially identical. Worth noting that we do not expect this trend to hold if one goes sufficiently beyond the 30th eigenvalue and eigenfunctions. Indeed, the approximation errors increases with λ, everything else being the same. We refer to [12] for details on the dependence on λ of the approximation errors for both eigenvalues and eigenfunctions.

On Table 4.3, we report the first thirty computed non-zero eigenvalues Λ_n and the number C_n of connected components of the nodal set of the associated eigenfunctions (U_{Λ_n}). These results, and their visualizations (see Figures 6 to 13), show

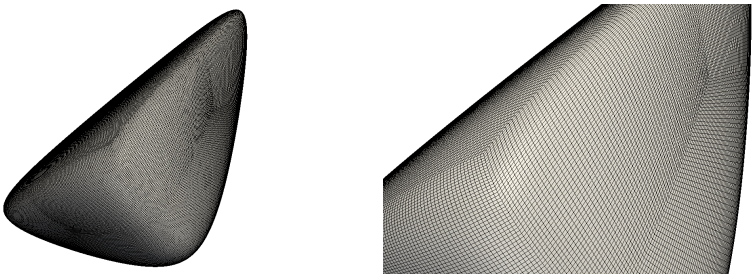

FIGURE 5. (Left) Subdivision Σ_2 made of $49,152$ cells; (Right) The quasi-uniformity of the subdivision is illustrated on a closer view of the same subdivision.

n	Λ_n	C_n	n	Λ_n	C_n
1	0.92141	1	16	15.2148	2
2	2.02604	1	17	15.321	2
3	2.77357	1	18	15.7848	3
4	3.14653	2	19	16.5163	4
5	4.77956	2	20	18.2277	5
6	5.87401	2	21	18.8446	4
7	6.32859	3	22	19.0875	2
8	7.36219	2	23	21.7026	3
9	7.90839	1	24	21.7879	4
10	8.63424	3	25	22.5371	3
11	10.0834	3	26	23.22	5
12	10.6645	4	27	24.9959	5
13	12.2416	4	28	25.5131	2
14	12.9988	2	29	25.9599	5
15	13.1605	4	30	26.678	2

TABLE 1. The first thirty non zero computed eigenvalues Λ_n and the number of connected components of the nodal set of the associated eigenfunctions C_n for the approximate surface Σ_2.

that these eigenvalues are of all of *multiplicity one*, and that the connected components of the nodal set of the associated eigenfunctions are *loops* which *do not intersect*. *We conjecture that these properties hold for all the pairs solution of the continuous eigenvalue problem* (2) *associated with* σ_2.

Remark 3 (Number of Connected Components)**.** The number of connected components of the nodal set is clearly a non-monotonic function of the rank of the associated eigenpair. Of course the numerical observations presented do not constitute a mathematical proof and in particular do not guarantee that this behavior will persist for larger n.

On the basis of the above results, we conjecture that the nodal lines corresponding to the eigenfunctions of the Laplace-Beltrami operator on Σ_2 *are non-self intersecting curves.*

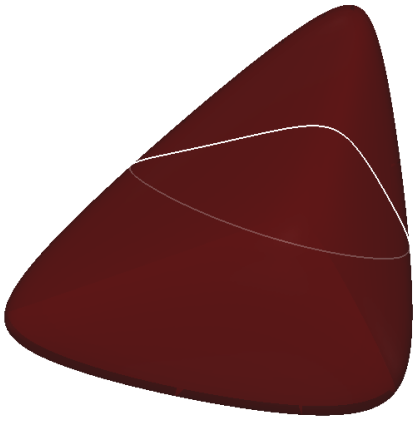

FIGURE 6. Surface Σ_2. Nodal lines of U_{Λ_1} ($C_1 = 1$).

n	Λ_n	n	Λ_n
1 & 2	18.5372 & 18.5373	16 & 17	191.484 & 191.484
3	30.0469	18 & 19	219.902 & 219.902
4 & 5	58.0478 & 58.048	20	233.552
6	65.996	21	241.473
7 & 8	79.5619 & 79.5621	22	243.475
9	113.05	23 & 24	249.798 & 249.798
10	115.814	25 & 26	290.066 & 290.066
11 & 12	136.067 & 136.067	27	316.146
13 & 14	149.791 & 149.791	28	320.665
15	152.58	29 & 30	346.091 & 346.091

TABLE 2. First thirty non-zero computed eigenvalues of the Laplace-Beltrami operator on Σ_3.

4.4. **Numerical Results for σ_3.** The approximation Σ_3 of σ_3 defined by (7) is constructed as for σ_2 described in Section 4.3. We computed the first thirty eigenpairs of the associated Laplace-Beltrami operator (with multiplicity taken into account). The first thirty computed eigenvalues of the Laplace-Beltrami operator associated with Σ_3 have been reported in Table 2.

We observed that for those eigenfunctions associated with multiple eigenvalues, the nodal lines do not intersect. In addition, the few ones for which the nodal lines intersect are of multiplicity one. We provide the approximate nodal lines associated

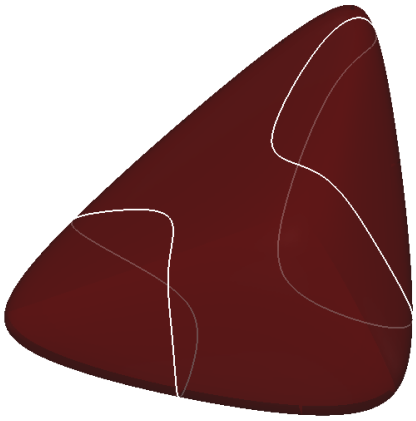

FIGURE 7. Surface Σ_2. Nodal lines of U_{Λ_5} ($C_5 = 2$).

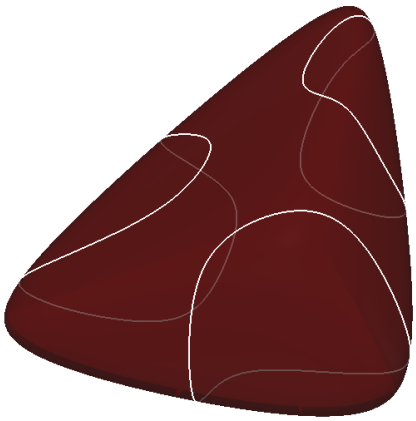

FIGURE 8. Surface Σ_2. Nodal lines of $U_{\Lambda_{10}}$ ($C_{10} = 3$).

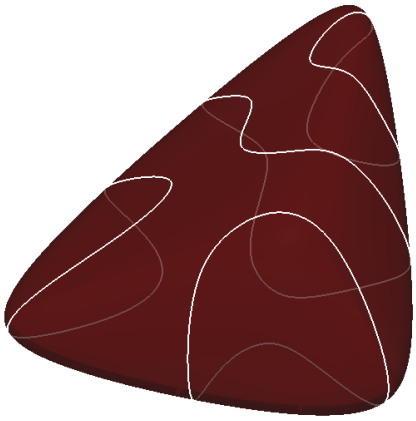

FIGURE 9. Surface Σ_2. Nodal lines of $U_{\Lambda_{15}}$ ($C_{15} = 4$).

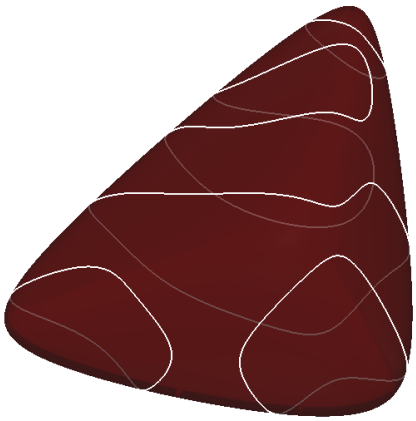

FIGURE 10. Surface Σ_2. Nodal lines of $U_{\Lambda_{20}}$ ($C_{20} = 5$).

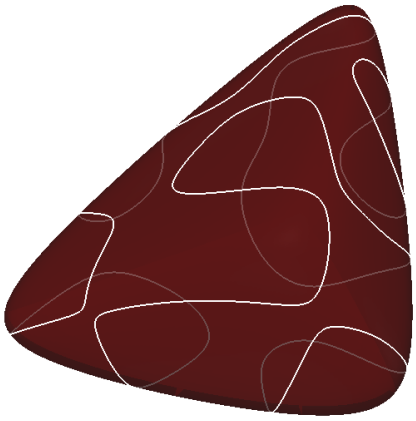

FIGURE 11. Surface Σ_2. Nodal lines of $U_{\Lambda_{25}}$ ($C_{25} = 3$).

with some nonzero eigenvalues in Figures 14 to 21. Notice that for the nodal lines for the 10th and 28th nonzero eigenfunctions intersect but not orthogonally as depicted in Figures 16 and 20.

On the basis of the properties of symmetry and of invariance by $\frac{3}{2}\pi$ and $\frac{3}{4}\pi$ rotations, the configuration of the nodal lines of the 10th eigenfunction was expected, but we did not anticipate the 28th. We never encountered eigenvalues of multiplicity more than 2. However, a similar pattern appears in the eigenproblem

$$-\Delta u = \lambda u \quad \text{in} \quad \Omega, \qquad u = 0 \quad \text{on} \quad \partial\Omega,$$

with $\Omega = (0,1)^2$. The related eigenvalues are all of the form $(m^2 + n^2)\pi^2$, with m and n two positive integers. The associated eigenfunctions, of unit norm in $L_2(\Omega)$ are given by

$$\{x, y\} \to \pm 2 \sin(m\pi x) \sin(n\pi y).$$

The first *triple* eigenvalue is the 31st one, namely $50\pi^2$, obtained for the values $\{5,5\}$, $\{7,1\}$ and $\{1,7\}$ of the pair $\{m,n\}$.

Acknowledgments. The authors would like to thank David Bao, Tony F. Chan, Monica Clapp, Fritz Foss, Ronald Hoppe, Patricia Saavedra for various comments and suggestions.

REFERENCES

[1] W. Bangerth, R. Hartmann, and G. Kanschat. deal.II – a general purpose object oriented finite element library. *ACM Trans. Math. Softw.*, 33(4):24/1–24/27, 2007.

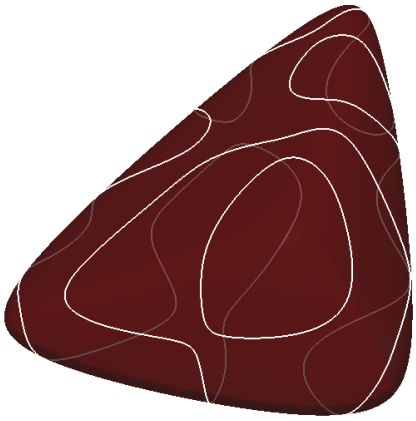

FIGURE 12. Surface Σ_2. Nodal lines of $U_{\Lambda_{28}}$ ($C_{28} = 2$). The nodal set of the 28th non constant eigenfunction consists of two curves only, one of them being pretty convoluted.

[2] A. Bonito, J.M. Cascón, P. Morin, and R.H. Nochetto. AFEM for geometric PDE: The Laplace-Beltrami operator. In *Analysis and Numerics of Partial Differential Equations*, volume 4, pages 257–306. Springer INdAM Series, 2013.

[3] A. Bonito and R.H. Nochetto. Quasi-optimal convergence rate of an adaptive discontinuous Galerkin method. *SIAM J. Numer. Anal.*, 48(2):734–771, 2010.

[4] A. Bonito and J.E. Pasciak. Convergence analysis of variational and non-variational multigrid algorithms for the Laplace-Beltrami operator. *Math. Comp.*, 81(279):1263–1288, 2012.

[5] A. Bonito and M.S. Pauletti. The step-38 tutorial progam: The laplace-beltrami operator. *http://www.dealii.org* .

[6] S.Y. Cheng. Eigenfunctions and nodal sets. *Comment. Math. Helv.*, 51(1):43–55, 1976.

[7] G. Dziuk. An algorithm for evolutionary surfaces. *Numer. Math.*, 58(6):603–611, 1991.

[8] F. J. Foss, II, R. Glowinski, and R. H. W. Hoppe. On the numerical solution of a semilinear elliptic eigenproblem of Lane-Emden type. I. Problem formulation and description of the algorithms. *J. Numer. Math.*, 15(3):181–208, 2007.

[9] F. J. Foss, II, R. Glowinski, and R. H. W. Hoppe. On the numerical solution of a semilinear elliptic eigenproblem of Lane-Emden type. II. Numerical experiments. *J. Numer. Math.*, 15(4):277–298, 2007.

[10] R. Glowinski and D.C. Sorensen. Computing the eigenvalues of the Laplace-Beltrami operator on the surface of a torus: a numerical approach. In *Partial differential equations*, volume 16 of *Comput. Methods Appl. Sci.*, pages 225–232. Springer, Dordrecht, 2008.

[11] V. Hernandez, J.E. Roman, and V. Vicente. SLEPc: A scalable and flexible toolkit for the solution of eigenvalue problems. *ACM Trans. Math. Software*, 31(3):351–362, 2005.

[12] R. Lai, Y. Shi, I. Dinov, T.F. Chan, and A.W. Toga. Laplace-Beltrami nodal counts: a new signature for 3D shape analysis. In *2009 IEEE International symposium on biomedical imaging: From nano to macro, Vols 1 and 2*, pages 694–697, 2009. IEEE Internaional Symposium on Biomedical Imaging - From Nano to Macro, Boston, MA, JUN 28-JUL 01, 2009.

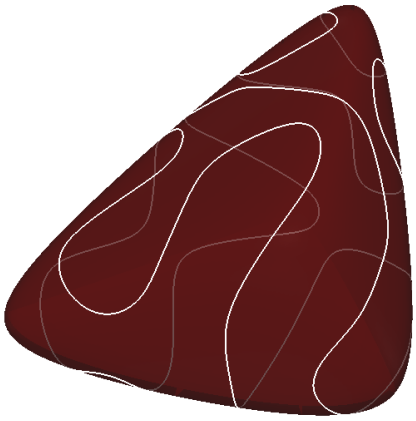

FIGURE 13. Surface Σ_2. Nodal lines of $U_{\Lambda_{30}}$ ($C_{30} = 2$). The nodal set of the 30th non constant eigenfunctions consists of two curves only, one of them being pretty convoluted.

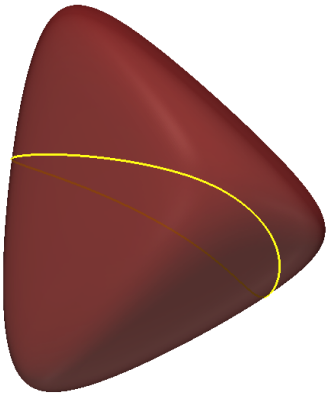

FIGURE 14. Surface Σ_3. Nodal line of U_{Λ_1} ($C_1 = 1$). The nodal line do not self intersect.

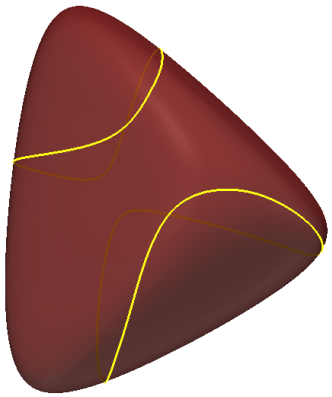

FIGURE 15. Surface Σ_3. Nodal lines of U_{Λ_5} ($C_5 = 2$). The nodal lines do not intersect.

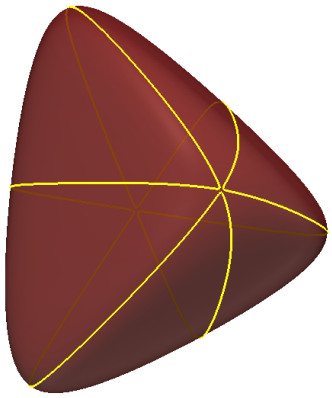

FIGURE 16. Surface Σ_3. Nodal lines of $U_{\Lambda_{10}}$ ($C_{10} = 1$). The nodal lines intersect.

[13] R. B. Lehoucq, D. C. Sorensen, and C. Yang. *ARPACK users' guide*, volume 6 of *Software, Environments, and Tools*. Society for Industrial and Applied Mathematics (SIAM), Philadelphia, PA, 1998. Solution of large-scale eigenvalue problems with implicitly restarted Arnoldi methods.

[14] K. Uhlenbeck. Generic properties of eigenfunctions. *Amer. J. Math.*, 98(4):1059–1078, 1976.

Received xxxx 20xx; revised xxxx 20xx.

E-mail address: bonito@math.tamu.edu
E-mail address: roland@math.uh.edu

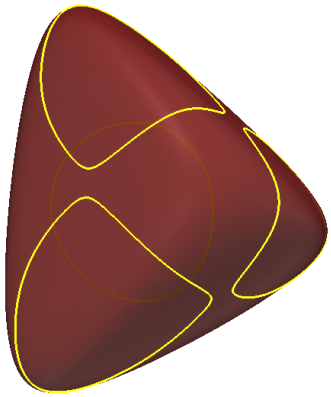

FIGURE 17. Surface Σ_3. Nodal lines of $U_{\Lambda_{15}}$ ($C_{15} = 4$). The nodal lines do not intersect.

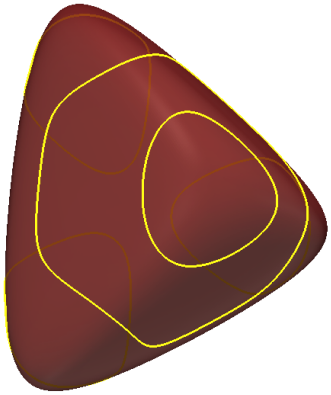

FIGURE 18. Surface Σ_3. Nodal lines of $U_{\Lambda_{20}}$ ($C_{20} = 5$). The nodal lines do not intersect.

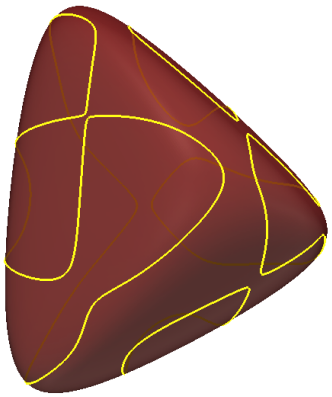

FIGURE 19. Surface Σ_3. Nodal lines of $U_{\Lambda_{25}}$ (not enough resolution to determine C_{25}).

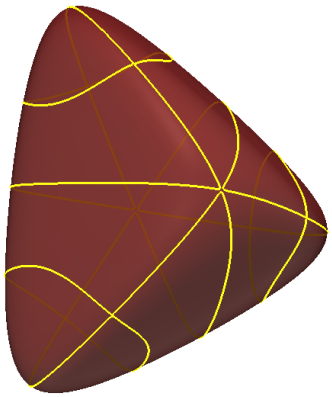

FIGURE 20. Surface Σ_3. Nodal lines of $U_{\Lambda_{28}}$ ($C_{28} = 1$). The nodal lines intersect.

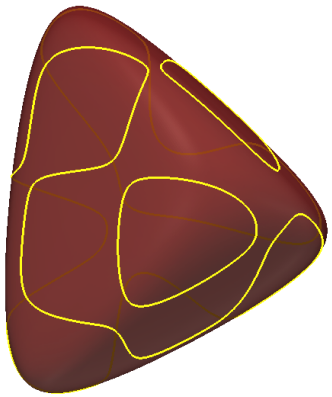

FIGURE 21. Surface Σ_3. Nodal lines of $U_{\Lambda_{30}}$ (not enough resolution to derermine C_{30}).